

Preface

Preface

Executive Committee

Executive Committee

Program Committee

Program Committee

Referees

Referees

Sponsoring Institutions

Sponsoring Institutions

Table of Contents

tocmark

ANIMAL+INSECT: improved cortical structure segmentation	1
<i>D. Louis Collins, Alex P. Zijdenbos, Wim F.C. Baaré and Alan C. Evans</i>	

ANIMAL+INSECT: improved cortical structure segmentation

D. Louis Collins¹ and Alex P. Zijdenbos¹ and Wim F.C. Baaré² and Alan C. Evans¹

¹ McConnell Brain Imaging Centre, Montréal Neurological Institute, McGill University, 3801 University St., Montréal, Canada H3A 2B4

`louis,alex,alan@bic.mni.mcgill.ca`

² Dept. Psychiatry, University Hospital Utrecht, Utrecht, the Netherlands
`wim@ni.azu.nl`

Abstract. An algorithm for improved automatic segmentation of gross anatomical structures of the human brain is presented that merges the output of a tissue classification process with gross anatomical region masks, automatically defined by non-linear registration of a given data set with a probabilistic anatomical atlas. Experiments with 20 real MRI volumes demonstrate that the method is reliable, robust and accurate. Manually and automatically defined labels of specific gyri of the frontal lobe are similar, with a Kappa index of 0.657.

1 Introduction

Quantitative analysis of neuro-anatomical or neuro-functional data often requires explicit regional identification of gross anatomical structures. Unfortunately, manual segmentation is time-consuming, subjective and error prone. Furthermore, inter- and intra-observer variability may reduce detectability of subtle differences when making comparisons. Automatic structure identification from medical images is a difficult task, due to the anatomical variability between subjects, differences in subject positioning (between patients and with respect to standard anatomical texts), the distinct physical properties measured by the imaging modalities, and variability of acquisition parameters such as slice thickness and pixel size.

It is important to note that we differentiate between *classification* and *segmentation*. We define segmentation to be the top-down regional parceling of an image into anatomically meaningful continuous groups of voxels; classification is defined to be the bottom-up (or data driven) labelling of individual voxels with a tissue class label without demanding spatial contiguity for a class of voxels. The image data represent only one measure (or a few measures in the case of multi-spectral data) concerning the underlying anatomy, and by itself is sufficient only for classification. Anatomically distinct regions of the brain are differentiated on the basis of histology, cyto-architecture, connectivity, cyto-chemistry or function. As such, data from external sources are required to constrain and guide the segmentation process.

These external data can be represented in at least two basic forms, and this distinction is used here as a basis to identify two main classes of methods that have been proposed to solve the segmentation problem for different applications. In the first, a symbolic mapping is created between features extracted from the image volume (usually small homogeneous regions) and a symbolic model of the anatomical structures to be segmented.

Expert rule-based systems are often used to achieve this mapping where anatomical knowledge is stored explicitly along with segmentation heuristics in semantic form such as an ‘if-then’ rule. Example of these procedures can be found in the work of Raya *et. al.* [1], Chen *et. al.* [2], Dellepiane *et. al.* [3], Arata and Dhawan [4, 5] and Davis *et. al.* [6]. Other algorithms do not explicitly employ if-then rules to drive the segmentation. Instead, anatomical constraints are implicitly incorporated into the procedure. Kaneda *et. al.* [7] use model-guided contour extraction and 3-D reconstruction to identify dilated ventricles in CT images. Anatomical constraints have also been used by Brummer [8, 9] to extract brain contours from MRI. Pathology (i.e., MS lesions) can be identified using similar techniques [10].

Registration-based segmentation procedures differ from those previously described, since they estimate a spatial transformation function that best maps features of one data set onto another pre-labelled volume that serves as an iconic model. These procedures are all based on the assumption that there exists a one-to-one mapping between the brain to be segmented and the one used as a model. In one of the first 2D examples, Broit *et. al.* [11] used elastically-constrained non-linear registration between a computed tomography (CT) image and a corresponding atlas slice. This work has been continued by Bajcsy *et. al.*, extended to 3D and reposed in a probabilistic formulation [12–14]. Miller *et. al.* also use a probabilistic formulation with physically based models [15–17] in order to segment individual brains by registering them to a target. We too have developed a registration-based segmentation procedure named ANIMAL (Automatic Nonlinear Image Matching and Anatomical Labeling) to automatically identify structures in the brain (described in more detail in section 2.4). It has been shown to successfully segment basal ganglia structures [18] but it has not been able to segment cortical structures satisfactorily (voxel-based overlap indices with manual segmentations have been typically around 40-50%). There are two reasons for this: i) there exists important variability in the topology of sulcal and gyral patterns cortex. For example, how should one account for the existence of a double Heschl’s Gyrus in a subject when the pre-labeled target has only one? This is an example of where the one-to-one relationship that ANIMAL depends on does not hold at the cortex¹. ii) the deformation field estimated by ANIMAL does not have the power to unfold the cortex of one brain and then refold it back onto a target brain. The deformation field is bandlimited and therefore does not have high enough frequencies to introduce (or remove) cortical folds

¹ Note that this problem affects not only ANIMAL, but all registration-based segmentation procedures. Even though fluid-based methods may recover a continuous mapping, point correspondence between model and model is ill-defined.

where needed. Still, the ANIMAL procedure is able to correctly identify structure location, position and smooth structure boundaries.

The procedure presented here addresses these problems. By merging the complementary information from ANIMAL’s non-linear deformation (i.e., low resolution region identification) with the output of a classification technique (i.e., voxel class labels), it is possible to accurately identify specific cortical structures from a subject’s MRI. The work presented here is most similar to that of Zachmann *et. al.* [19], where an iconic model (represented by a voxelated volume, where the value in each voxel represents the probability of existence of a structure) is used for identification of the different fluid spaces of the brain. The work here is different in that it is fully 3D, uses non-linear registration (instead of linear), and is applied to the entire cerebral volume including not only the cerebrospinal fluid (CSF) filled spaces, but deep brain structures and cortical gyri and sulci as well.

2 Methods

2.1 Stereotaxy

The methodology presented here is highly dependent on the notion of stereotaxic space, i.e., a standardized brain-based coordinate system that yields a method of identification of structure location and position so that regions of interest can be compared between brains using standard coordinates. Like many groups in brain mapping research, we have selected to use a coordinate system similar to that defined by Talairach [20] with the origin placed at the anterior commissure, the x -axis running from left to right, the y -axis running from posterior to anterior and the z -axis running from inferior to superior.

When image volumes are transformed into this space and resampled on the same voxel grid such that all brains have the same orientation and size, voxel-by-voxel comparisons across data volumes from different populations are possible, since each voxel (i, j, k) corresponds to the same (x, y, z) point in the brain-based coordinate system. The transformation to this coordinate system also provides a means for enhancement of functional signals by averaging images in this space [21]. This paradigm allows information (anatomical, metabolic, electrophysiological, chemical, architectonic) from different brains to be spatially organized and catalogued by mapping all brains into the same coordinate system [22]. Finally, in the original Talairach spirit, the coordinate corresponding to a particular structure, as defined by an atlas in this coordinate system, can be used to predict its location in a subject’s brain volume when mapped into the same space. However, normal anatomical morphometric variability limits this predictive value since there remains variability in structure position even after linear transformation.

We represent this variability by a statistical probability anatomy maps (SPAM) [23]. By definition, the SPAM for any given structure is a volumetric data set sampled in stereotaxic space, where the value at each voxel position represents

the probability of existence of that structure at that location within the brain-based coordinate system. At each voxel, the probability is proportional to the number of volumes containing the structure label, divided by the total number of volumes. For example, SPAMs can be created with voxel-by-voxel averaging of label volumes from tissue classified data from many subjects to yield spatial priors that can be used in classification procedures. Here the SPAMs are created from the segmented structure labels from many subjects (see section 2.5) and used as prior anatomical model information to drive the segmentation.

2.2 MRI preprocessing

A number of processing steps are required to achieve segmentation. We have combined preprocessing steps (image intensity non-uniformity correction [24]), linear registration (ANIMAL in linear mode [25]) and resampling into stereotaxic space, cortical surface extraction (Multiple surface deformation or MSD [26, 27]), tissue classification (INSECT [28]), and non-linear registration (ANIMAL in non-linear mode [18]) into a processing pipeline. These are represented schematically in Fig. 1. Since the ANIMAL and INSECT procedure are merged to improve segmentation, the new procedure is termed ANIMAL+INSECT. After running this pipeline, a subject's MRI volume can be visualized in stereotaxic space with its corresponding tissue labels, anatomical structure labels and cortical surface — all in 3D. The following sections describe the classification (INSECT) and non-linear registration (ANIMAL) procedures in more detail.

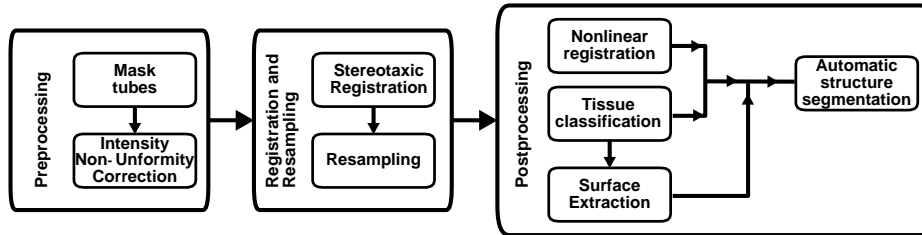


Fig. 1. Processing pipeline

All MRI data are processed through the pipeline shown above. After preprocessing to correct for intensity non-uniformity, the data are linearly registered into stereotaxic space and resampled onto a 1mm isotropic grid. The resulting volume is automatically classified into GM, WM, and CSF components and the cortical surface is automatically extracted. The non-linear transformation to stereotaxic space is used to warp the standard probabilistic atlas onto the classified data, defining structures by masking tissue classes. The cortical surface is used to mask non-brain from cerebral structures.

2.3 INSECT

After image intensity non-uniformity correction, stereotaxic registration and re-sampling, the classification strategy used by INSECT relies on a standard feed-forward error-backpropagation artificial neural network (ANN). Since after re-sampling an (x,y,z) location in the image lattice corresponds to the same physical (brain) location in all MRI modalities, the intensity values of all MRI modalities at that location are used as the ANN inputs. As such, the number of ANN input nodes is equal to the number of MRI modalities, whereas the number of output nodes is equal to the number of tissue classes (typically white matter, gray matter, CSF, and background). The ANN is fully connected between layers, and contains one hidden layer with 10 nodes. Training of the network is accomplished using a collection of fixed stereotaxic coordinates, derived from the SPAMs (or probability maps, see section 2.1) of WM, GM, and CSF. Based on these SPAMs, any spatial location included in the training set belongs to one of the three tissue classes with a minimum likelihood of 90%. The MRI intensity values of the subject’s MRI acquisition at these locations are used as training input to the ANN, with the corresponding tissue class label as the target output. After training, the ANN is used to classify each voxel of the subject data set into WM, GM, or CSF.

2.4 ANIMAL

Identification of individual brain regions, such as the caudate nucleus, planum temporale or superior frontal gyrus, faces two major problems. First, while anatomists may generally agree where a structure is located, there is often no consensus on exactly which part of the structure should be included or excluded. Secondly, the manual labelling process is both time-consuming and the position identified of chosen boundary is subjective, and dependent on the level and contrast of the image displayed. To address these difficulties we have developed ANIMAL, an algorithm to perform this labelling automatically in 3D [18].

The ANIMAL algorithm deforms one MRI volume to match another, previously labelled, target MRI volume. It builds up a 3D non-linear deformation field in a piecewise linear fashion, recursively fitting local spherical neighbourhoods. Each local neighbourhood from one volume is translated to achieve an optimal match within the other volume. The local neighbourhoods are arranged on a 3-D grid to fill the volume and each grid node moves within a range defined by the grid spacing. The algorithm is applied iteratively in a multi-scale hierarchy. At each step image volumes are convolved with a 3D Gaussian blurring kernel where blurring and neighbourhood size (sphere diameter) are reduced after each stage. Local neighbourhood fit is measured by correlation of the blurred image intensities. Initial fits are obtained rapidly since at lower scales, only gross distortions are considered, but later iterations at finer scales accommodate local differences at the price of increasing computational cost. Anatomical segmentation is achieved by transforming labels from the second (target) volume onto the

first volume, via the inverse of spatial mapping of the 3D deformation field (see Fig. 5-c for an example of an ANIMAL segmentation).

This method has the important advantage that it is atlas independent, since the labels do not take part in the fitting process. In fact, multiple atlases defined for different applications or by different anatomists can co-exist on the target volume, and each one can be mapped through the non-linear transformation without recomputation of the latter.

2.5 ANIMAL+INSECT

In the standard application of ANIMAL, the target is an MRI volume from a single subject where all of the voxels within the volume have been anatomically labelled by a neuroanatomist to form an atlas [29]. In the ANIMAL+INSECT paradigm described here, the target is an voxel-by-voxel intensity average of 305 MRI volumes, where each volume was automatically registered and resampled in stereotaxic space [30]. The atlas used for segmentation was created by averaging anatomical labels from 152 subjects young normal subjects, collected as part of the ICBM project [31].

Probabilistic atlas There are a number of problems associated with an anatomical atlas that is based on a single subject. For example, even though the subject may be normal, certain brain regions may represent an extreme of the normal distribution. Also, the use of a single brain atlas does not contain any notions of anatomical variability, so it is impossible to evaluate the normality of shape, size or position of specific structures from other subjects by comparing them with the atlas. Finally, only one cortical topology (sulcal/gyral pattern) is represented even though large variability is known to exist [32]. Since all registration-based segmentations strategies (ANIMAL included) are based on the assumption that there exists a 1-to-1 homology for all structures between source and target brains, these strategies are undefined and may fail when this correspondence does not exist, especially at the cortex.

Many of the problems listed above are addressed by using a probabilistic atlas, or SPAM, created from the labellings of a large ensemble of normal subjects [23]. The SPAM atlas used here models the anatomical variability of shape, size and topology of 91 gross anatomical structures, where each structure is represented by a SPAM volume in stereotaxic space (see section 2.1). The ANIMAL+INSECT segmentation paradigm requires that the atlas labels be transformed from the target space and resampled onto the subject's MRI volume. Resampling a large number of SPAM volumes is inefficient, since only the label of the most likely structure at each voxel position need be transferred to the subject's volume for masking. Therefore, a max-probability atlas (MPA) was created in the target space, where only the label of the most probable structure is stored at each voxel. This volume is created once by traversing the stereotaxic volume, voxel-by-voxel, and storing only the label of the SPAM with the highest probability at that voxel.

In practice, labelled data from large number of subjects is needed to create the atlas. Ideally, manual segmentations of all atlas structures on all subjects should be used. Unfortunately manual identification is very time consuming (e.g., 1 man-month required to segment the thalamus on 200 subjects [33]), making the ideal situation unrealistic. Here, as proof of principal, the standard ANIMAL [18] procedure was used with a gross anatomical atlas containing 91 structures [29] to segment 150 data sets of young normal adults [34]. Validations of the ANIMAL procedure have demonstrated that on average, automatic segmentations are comparable to manual labellings for basal ganglia [18] and cortical gyri² [35], making this solution only slightly less than ideal. These 150 segmentations were used to create 91 SPAM volumes that were in turn used to produce the MPA shown in Fig 3. In addition, three other MPA models were created from 1) the set of 71 grey matter SPAMs to create a gMPA, 2) the set of 16 white matter SPAMs to create a wMPA and 3) the set of 4 CSF SPAMs to create a vMPA (*v* for ventricular).

Merge method Application of ANIMAL, using the MNI305 intensity average target and the corresponding MPA results in a *customized maximum probabilistic atlas* (c-MPA) for the given subject (see Fig. 4). This paradigm is similar to the typical use of the Talairach atlas in brain mapping for structure interpretation and localization. The major advantage is that the customized atlas indicates the most likely structure label for each voxel for a particular subject given anatomical variability of a normal population, instead of only a structure label of the single target brain. The ANIMAL+INSECT methodology makes a further improvement by incorporating tissue class information derived from the subject in question in the following manner.

After the three c-MPA models corresponding to GM, WM and CSF are warped and resampled, they are used as masks to assign labels to regions of the corresponding tissue types classified by INSECT. The c-gMPA is applied to the GM tissue class to identify the gyri of the different cerebral lobes, basal ganglia structures and the thalamus. The c-wMPA is applied to the WM tissue class to label the corpus collosum, the anterior and posterior limbs of the internal capsule and the WM voxels belonging to the lobes. In the same fashion, the c-vMPA is applied to the CSF tissue class to segment the lateral, third and fourth ventricles. Note that while the c-MPAs actually overlap and thus may yield several different labels for a given voxel, only the c-MPA label corresponding to the voxel's tissue is applied. In the same manner, partial volume effects may be accounted for if the classification procedure outputs continuous (instead of discrete) data. For example, sulcal CSF can be labelled as such with the c-vMPA, even though the classifier outputs CSF voxels with a magnitude less than 1.0.

Some cortical SPAMs extend past the inner table of the skull and may extend into the scalp with a very low (but non-null) probability, since there are no other

² It is interesting to note that while individual cortical structure labellings may be in error, SPAMs generated by averaging either manual or automatic labellings are very similar.

cerebral structure SPAMs that will compete for the maximum probability label. When the original MPA is created, these extra voxel labels remain and will erroneously apply a cortical label to voxels located in the skull or scalp that were classified as GM or WM. In order to remove these incorrect labels, the cortical surface extracted by MSD is used to create a brain mask that is applied against the label volume.

Some structures cannot be segmented using only the method described above. For example, in the T1-weighted volumes from the ICBM data base, the medial half of the thalamus is usually classified as GM, while the lateral half is classified as WM and cannot be distinguished from the adjacent white matter of the posterior limb of the internal capsule. In this case, it is impossible to apply a regional mask to a single tissue class to extract and label the structure. Therefore, some structure-specific segmentation rules are required. For the thalamus, the medial border is easily defined by masking the GM tissue class with the c-gMPA. The definition of the lateral border is completely model-based using the standard ANIMAL(-only) segmentation technique and is equal to the lateral border of the thalamus in the cMPA. Similar rules are used for the head of the caudate nucleus, putamen and globus pallidus. Once these structures are segmented, their labels are overlaid on top of the previous segmentation result, overwriting any labels already specified by the initial cMPA masking process.

3 Experiments and Results

3.1 MRI acquisition

The data used for the experiments described below were acquired as part of the International Consortium for Brain Mapping (ICBM) project, a Human Brain Mapping funded research project with the goal of building a probabilistic atlas of human neuro-anatomy [31]. T1-weighted MRI volumes from 152 young normal volunteers (86 male, 66 female, age 24.6 ± 4.8) were acquired using a 3-D spoiled gradient-echo acquisition with sagittal volume excitation (TR=18, TE=10, flip angle=30°, 140-180 sagittal slices). As described below in section 3, frontal lobe gyri were manually identified on twenty of these volumes.

3.2 Comparison of segmentations

Figure 5 shows a comparison of an ANIMAL-only segmentation, an ANIMAL+INSECT segmentation and a manual segmentation. Not only is the ANIMAL+INSECT segmentation improved at the cortex, where some grey-matter regions were missed with the standard ANIMAL technique, the segmentation of the lateral ventricles is much better as well. Where the ANIMAL technique overestimated the size of the ventricle, the ANIMAL+INSECT is in complete agreement with the MRI anatomy and with the expert's labelling. Note that there remain some discrepancies between the ANIMAL+INSECT and the manual segmentations - especially at the boundaries between gyri.

In order to determine how well the segmentation procedure works in general, we used manually segmented labels of gyri of the frontal lobes and compared these to automatic labellings.

3.3 Manual labelling

In each hemisphere, the gray matter of five pre-frontal regions (superior, medial and inferior frontal gyrus, the anterior cingulate gyrus and the orbito-frontal gyri) were labelled by hand. The voxels for each structure were manually identified by voxel painting using *Display*, a computer program developed in our lab [36] that shows four 2D orthogonal slices (transverse, coronal, sagittal and user-defined oblique) through the volume with arbitrary pan, zoom and intensity mapping on each slice. Display also includes a 3D graphics window that is capable of displaying 3D geometric objects such as the cortical surface. The cursor can be placed in any of the 2D or 3D windows, and its position is simultaneously updated in the other views. Voxel labels are painted on any of three orthogonal views with simultaneous update in the other two. Cortical landmarks such as the precentral, superior and inferior frontal, cingulate, fronto-orbital, fronto-marginal and superior rostral sulci are identified in the 3D window and are used to guide the manual segmentation. Manual segmentation of the ten gyri listed above required approximately 10-15 hours per subject.

3.4 Automatic labelling

Qualitatively, the images in Fig 2 demonstrate that the automatic labellings of the left superior frontal gyrus are very similar to the manual segmentations. In fact, the grey-white border and grey-CSF borders are very similar. In some cases however, the ANIMAL+INSECT method includes the opposite sulcal bank in the gyral labels.

In order to compare the two methods quantitatively, we have used a similarity measure first proposed by Dice [37]. As shown by Zijdenbos [38], this measure is a variant of the standard chance-corrected Kappa (κ) coefficient first developed by Cohen [39]. This measure is the same as κ when the background is infinitely large.

When averaged over the 20 segmentations, the mean and standard deviation of the κ variant is 0.657 ± 0.037 . In order to interpret this value and put it into context, the right-most image on the third row of Fig 2 has a value of 0.728 (best κ value in this experiment), while the third image in the top row has a value of 0.573 (worst κ value). Finally, the labelling of the superior frontal gyrus from a single subject was deliberately dilated by one voxel, and the κ variant was evaluated between on the original and dilated labelling, yielding 0.725. Dilating by 2 voxels yields 0.593.

4 Discussion

We have presented an improved method for automatic segmentation of brain structures by merging the complementary information from ANIMAL’s non-linear deformation regional identification with the output of INSECT’s classification technique. The procedure presented here is completely automatic and therefore fully objective and applicable to large ensembles of brain volumes. While the new procedure uses two algorithms that were developed at the Montreal Neurological Institute, the new improved segmentation method is not dependent on these particular methods. In fact, any classification method that differentiates tissue types and any non-linear registration method may be merged to maximize the complementary information of both techniques. Since INSECT yields high resolution structure information, it is no longer necessary to run ANIMAL to fine resolutions, thus providing a considerable improvement in speed. In fact, running times are reduced from approximately 10 hours for estimation of the high resolution non-linear fit to less than 2 hours, including both classification and low-resolution warping.

The qualitative results shown in Fig 2 demonstrate that the ANIMAL+INSECT methodology can segment individual gyri from MRI data. While the quantitative measures presented here are not as high as we would like, we are currently working on estimating intra- and inter-observer variability estimates to put these values into context.

At least three methodological problems remain for future work: 1) In their current form, the cortical SPAMs do not explicitly represent multiple topological patterns that exist for cortical gyri. We plan to use an atlas that contains multiple SPAM representations for specific cortical regions, where each SPAM corresponds to a given cortical pattern for that region. 2) Structures that have a high anatomical variability are represented by SPAMs whose size is smaller than their true average size. These structures must be segmented using a model-only method, similar to those described above for the segmentation of the thalamus, caudate, putamen and globus pallidus. 3) Surface data, extracted by MSD, will be used to refine over-defined cortical regions (e.g., where the opposite sulcal bank is included in the segmentation of a gyrus). By using the surface information, it will be possible to separate small disconnected regions on the cortical surface, and then correct the gyral labelling in 3D.

Acknowledgments

The authors would like to express their appreciation for support from the Human Frontier Science Project Organization, the Canadian Medical Research Council (SP-30), the McDonnell-Pew Cognitive Neuroscience Center Program, the U.S. Human Brain Map Project (HBMP), NIMH and NIDA. W.F.C.Baaré was supported by the Netherlands Organization for Scientific Research and the Foundation “De Drie Lichten” in the Netherlands. This work forms part of a continuing project of the HBMP-funded International Consortium for Brain Mapping (ICBM) to develop a probabilistic atlas of human neuroanatomy.

References

1. S. P. Raya. Low-level segmentation of 3D magnetic resonance brain images - a rule based system. *IEEE Transactions on Medical Imaging*, 9(3):327–337, 1990.
2. L.-S. Chen and M. R. Sontag. Representation, display and manipulation of 3D digital scenes and their medical applications. *Computer Vision, Graphics, and Image Processing*, 48:190–216, 1989.
3. S. Dellepiane, S. B. Serpico, and G. Vernazza. Approximate reasoning and knowledge in NMR image understanding. In *8th International Conference on Pattern Recognition*, pages 943–946, Paris, France, October 1986. IEEE.
4. L. Arata, A. P. Dhawan, J. Broderick, and M. Gaskil. Model-based analysis of MR images of the brain. *IEEE Engineering in Medicine and Biology*, 13(3):1331–1332, 1991.
5. A. P. Dhawan and L. Arata. Knowledge-based multi-modality three-dimensional image analysis of the brain. *American Journal of Physiologic Imaging*, 7(3-4):210–9, Jul-Dec 1992.
6. D. N. Davis and C. J. Taylor. A blackboard architecture for automating cephalometric analysis. *Med Inf (Lond)*, 16(2):137–49, Apr-Jun 1991.
7. Y. Kaneda, S. Fujii, Y. Kobashiri, M. Yoshirda, and M. Matsuo. Pattern recognition and three dimensional construction from CT images. In *Proceedings of the International Conference on Cybernetics and Society*, pages 281–284, Tokyo and Kyoto, Japan, Nov 3-7 1978. IEEE.
8. M. E. Brummer. Hough transform detection of the longitudinal fissure in tomographic head images. *IEEE Transactions on Medical Imaging*, 10(1), Mar. 1991.
9. M. E. Brummer, R. M. Mersereau, R. L. Eisner, and R. R. J. Lewine. Automatic detection of brain contours in MRI data sets. In A. C. F. Colchester and D. J. Hawkes, editors, *Information Processing in Medical Imaging*, page 188, Wye, UK, July 1991. IPMI.
10. I. Kapouleas. Automatic detection of white matter lesions in magnetic resonance brain images. *Comput Methods Programs Biomed*, 32(1):17–35, May 1990.
11. C. Broit. *Optimal registration of deformed images*. PhD thesis, University of Pennsylvania, Philadelphia, 1981.
12. R. Bajcsy and C. Broit. Matching of deformed images. In *Proceedings of the 6th International Conference on Pattern Recognition*, pages 351–353, Munich, Germany, Oct 19-22 1982. IEEE.
13. R. Dann, J. Hoford, S. Kovacic, M. Reivich, and R. Bajcsy. Three-dimensional computerized brain atlas for elastic matching: Creation and initial evaluation. In *Medical Imaging II*, pages 600–608, Newport Beach, Calif., February 1988. SPIE.
14. J. C. Gee, L. LeBriquer, and C. Barillot. Probabilistic matching of brain images. In Y. Bizais and C. Barillot, editors, *Information Processing in Medical Imaging*, Ile Berder, France, July 1995. IPMI, Kluwer.
15. M. I. Miller, Y. Amit G. E. Christensen, and U. Grenander. Mathematical textbook of deformable neuroanatomies. *Proceedings of the National Academy of Sciences*, 90(24):11944–11948, 1990.
16. G. E. Christensen, R. D. Rabbitt, and M. I. Miller. 3D brain mapping using a deformable neuroanatomy. *Physics in Med and Biol*, 39:609–618, 1994.
17. G. E. Christensen, R. D. Rabbitt, and M. I. Miller. Deformable templates using large deformation kinematics. *IEEE Transactions on Image Processing*, 5(10):1435–1447, 1996.

18. D. L. Collins, C. J. Holmes, T. M. Peters, and A. C. Evans. Automatic 3D model-based neuroanatomical segmentation. *Human Brain Mapping*, 3(3):190–208, 1995.
19. H. H. Zachmann. Interpretation of cranial MR-images using a digital atlas of the human head. *IEEE Transactions on Medical Imaging*, pages 99–110, 1991.
20. J. Talairach and P. Tournoux. *Co-planar stereotactic atlas of the human brain: 3-Dimensional proportional system: an approach to cerebral imaging*. Georg Thieme Verlag, Stuttgart, New York, 1988.
21. Peter T. Fox, Mark A. Mintun, Eric M. Reiman, and Marcus E. Raichle. Enhanced detection of focal brain responses using intersubject averaging and change-distribution analysis of subtracted PET images. *Journal of Cerebral Blood Flow and Metabolism*, 8:642–653, 1988.
22. P. T. Fox, S. Mikiten, G. Davis, and J. L. Lancaster. BrainMap: A database of functional brain mapping. In R. W. Thatcher, M. Hallett, T. Zeffiro, E. R. John, and M. Heurta, editors, *Functional Neuroimaging, technical foundations*, pages 95–105. Academic Press, San Diego, Ca., 1994.
23. A. C. Evans, D. L. Collins, and C. J. Holmes. Automatic 3D regional MRI segmentation and statistical probability anatomy maps. In T Jones, editor, *Quantification of Brain Function: Tracer kinetics and image analysis in brain PET*, pages 123–130. 1995.
24. J. G. Sled, A. P. Zijdenbos, and A. C. Evans. A non-parametric method for automatic correction of intensity non-uniformity in MRI data. *IEEE Transactions on Medical Imaging*, 17(1), Feb. 1998.
25. D. L. Collins, P. Neelin, T. M. Peters, and A. C. Evans. Automatic 3D inter-subject registration of MR volumetric data in standardized talairach space. *Journal of Computer Assisted Tomography*, 18(2):192–205, March/April 1994.
26. D. MacDonald, D. Avis, and A. C. Evans. Multiple surface identification and matching in magnetic resonance images. In *Proceedings of Conference on Visualization in Biomedical Computing*. SPIE, 1994.
27. D. MacDonald. *Identifying geometrically simple surfaces from three dimensional data*. PhD thesis, McGill University, Montreal, Canada, December 1994.
28. A. P. Zijdenbos, A. C. Evans, F. Riahi, J. Sled, J. Chui, and V. Kollokian. Automatic quantification of multiple sclerosis lesion volume using stereotaxic space. In *Proceedings of the 4th International Conference on Visualization in Biomedical Computing, VBC '96*, pages 439–448, Hamburg, September 1996.
29. N. J. Kabani, D. L. Collins, and A. C. Evans. A 3D neuroanatomical atlas. In A.C. Evans, editor, *4th International Conference on Functional Mapping of the Human Brain*, Montreal, June 1998. Organization for Human Brain Mapping. submitted.
30. A. C. Evans, D. L. Collins, and B. Milner. An MRI-based stereotactic atlas from 250 young normal subjects. *Soc. Neurosci. Abstr.*, 18:408, 1992.
31. JC Mazziotta, AW Toga, AC Evans, P Fox, and J Lancaster. A probabilistic atlas of the human brain: theory and rationale for its development. the international consortium for brain mapping. *NeuroImage*, 2(2):89–101, 1995.
32. M. Ono, S. Kubik, and C. D. Abernathy. *Atlas of Cerebral Sulci*. Georg Thieme Verlag, Stuttgart, 1990.
33. J. Absher. A probabilistic atlas of the thalamus. Technical report, McConnell Brain Imaging Centre, Montreal Neurological Institute, McGill University, Montreal, Sept 1993.
34. D. L. Collins, N. J. Kabani, and A. C. Evans. Automatic volume estimation of gross cerebral structures. In A.C. Evans, editor, *4th International Conference on Functional Mapping of the Human Brain*, Montreal, June 1998. Organization for Human Brain Mapping. abstract no. 702.

35. W. F. C. Baaré, D. L. Collins, N. Kabani, D. MacDonald, C. Liu, M. Petrides, R. S. Kwan, and AC Evans. Automated and manual identification of frontal lobe gyri. In *Third International Conference on Functional Mapping of the Human Brain*, volume 5, page S348, Copenhagen, May 1997. Human Brain Map.
36. D. MacDonald. Display: a user's manual. Technical report, McConnell Brain Imaging Centre, Montreal Neurological Institute, McGill University, Montreal, Sept 1996.
37. L. R. Dice. Measures of the amount of ecologic association between species. *Ecology*, 26(3):297–302, 1945.
38. A. P. Zijdenbos, B. M. Dawant, R. A. Margolin, and A. C. Palmer. Morphometric analysis of white matter lesions in MR images: Method and validation. *IEEE Transactions on Medical Imaging*, 13(4):716–724, December 1994.
39. J. Cohen A coefficient of agreement for nominal scales. *Educational and Psychological Measurements*, 20:37–46, 1960.

Fig. 2. Segmentation of the Superior Frontal Gyrus

These images compare the manual (left) and automatic (right) segmentations of the left superior frontal gyrus on coronal slices from 20 subjects.

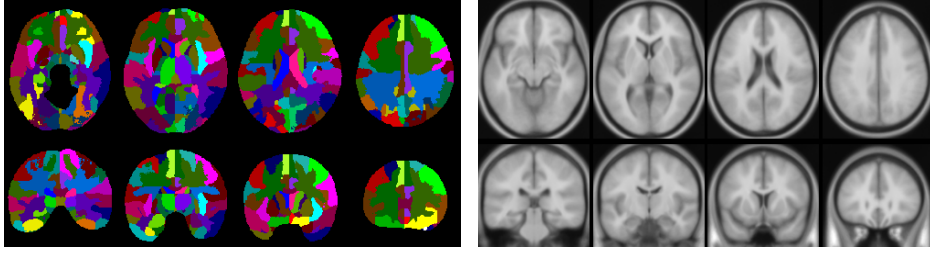


Fig. 3. Max-probability atlas

These images show slices through the maximum probability atlas (left) and the corresponding slices through the ICBM150 T1-weighted average brain (right).

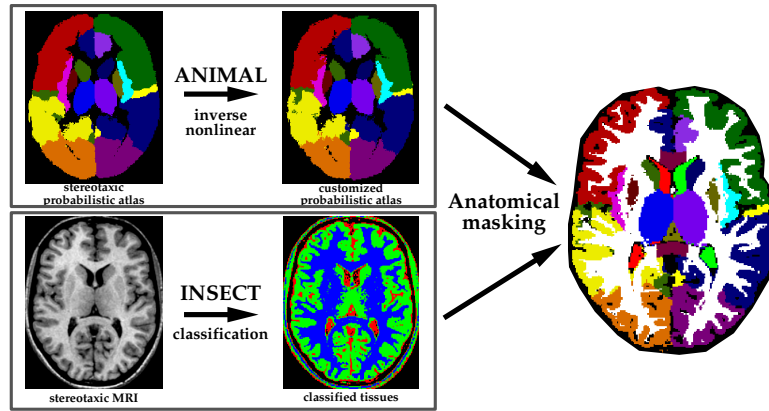


Fig. 4. Schematic of ANIMAL+INSECT merge.

The non-linear transformation required to customize the stereotaxic MPA for the subject is estimated by ANIMAL. The subject's MRI is classified into WM, GM and CSF classes by INSECT. The classified data are masked by the regions in the c-MPA to segment regions on the subject's MRI volume.

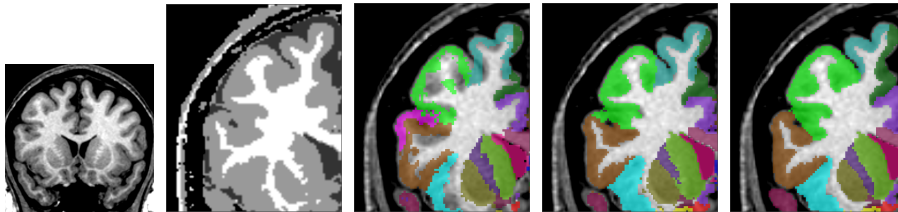


Fig. 5. ANIMAL-only vs ANIMAL+INSECT

(Left to right) Coronal slice through original MRI volume; typical zoomed result (upper left quadrant) result of INSECT classification; of ANIMAL-only segmentation; of ANIMAL+INSECT segmentation; or manual segmentation. Note how the ANIMAL+INSECT result improves segmentation at the cortex and the ventricles and agrees with the expert labelling.